

Article

Synthesis and Electrical Properties of a New Bipolar Material Using Spacer Moiety

Seunghyeon Jo [†], Sangwook Park [†], Hyukmin Kwon, Hayoon Lee, Kiho Lee  and Jongwook Park ^{* }

Integrated Engineering, Department of Chemical Engineering, Kyung Hee University, Yongin-si 17104, Gyeonggi, Republic of Korea; darl405@khu.ac.kr (S.J.); pswook@khu.ac.kr (S.P.); hm531@khu.ac.kr (H.K.); kssarang1@khu.ac.kr (H.L.); kiholee@khu.ac.kr (K.L.)

* Correspondence: jongpark@khu.ac.kr; Tel.: +82-10-8759-8485

[†] These authors contributed equally to this work.

Abstract: To develop a deep-blue emitter, a molecule with bipolar characteristics was designed as a donor-spacer-acceptor type, in which 9-(4-(4,6-diphenyl-1),3,5-triazin-2-yl)-2,5-dimethylphenyl)-9H-carbazole (DTPCZ)—with carbazole as an electron donating group and a diphenyl triazine moiety as an electron accepting group—was successfully synthesized. The photoluminescence (PL) maxima of DTPCZ were 421 nm in the solution state and 425 nm in the film state, indicating emission in the deep-blue region. DTPCZ also exhibited high thermal stability, with a degradation temperature of 349 °C. To confirm the electroluminescence (EL) characteristics, DTPCZ was applied as a dopant at 10, 20, and 30 wt% in a blue-fluorescent organic light-emitting diode (OLED) device. The highest efficiency was achieved using the 20 wt% doped device, with a current efficiency of 1.2 cd/A, an external quantum efficiency of 2.3%, and a Commission Internationale de l’Eclairage proceedings y -value of 0.06. Thus, deep-blue emission could be realized in the film state. These molecular design strategies can be applied to various fields, such as organic semiconductors.

Keywords: organic light-emitting diodes; blue emission; bipolar; charge transfer



Citation: Jo, S.; Park, S.; Kwon, H.; Lee, H.; Lee, K.; Park, J. Synthesis and Electrical Properties of a New Bipolar Material Using Spacer Moiety. *Appl. Sci.* **2024**, *14*, 3593. <https://doi.org/10.3390/app14093593>

Academic Editor: John Xiupu Zhang

Received: 5 April 2024

Revised: 19 April 2024

Accepted: 22 April 2024

Published: 24 April 2024



Copyright: © 2024 by the authors. Licensee MDPI, Basel, Switzerland. This article is an open access article distributed under the terms and conditions of the Creative Commons Attribution (CC BY) license (<https://creativecommons.org/licenses/by/4.0/>).

1. Introduction

Since the introduction of organic light-emitting diode (OLED) technology in 1987 by Dr. Tang, researchers have focused on improving the efficiency and lifetime of OLED displays while reducing manufacturing costs [1]. OLEDs offer many advantages in terms of their light weight, thin panel construction, wide viewing angle, high color saturation, and fast response time. These properties have led to their use in numerous products, including smartphones, televisions, and wearable devices. In an attempt to achieve optimal full-color display, considerable effort has been expended regarding the identification of red-, green-, and blue-emitting materials with excellent performance [2]. In particular, there is an increasing need for deep-blue materials that satisfy the Commission Internationale de l’Eclairage (CIE) coordinates (0.14, 0.08) for deep blue, which was established by the National Television System Committee for OLED televisions and applications [3,4]. Thus, there is active research regarding high-efficiency deep-blue dopants with bipolar characteristics. In particular, conjugated materials with such bipolar characteristics are crucial for enhancing charge transport and the efficiency of charge transfer in organic semiconductors.

Emitting materials with bipolar characteristics are commonly composed of donor-acceptor structures. In these bipolar structures, it is difficult to realize deep blue because intramolecular charge transfer between donors and acceptors effectively reduces the band gap. However, deep blue can be achieved using the following three strategies (i–iii): (i) enhancement of steric hinderance between donors and acceptors; (ii) maintenance of an appropriate distance between the two moieties using a donor-spacer-acceptor type; and/or (iii) reduction of electron donating and accepting capacities [5–8]. Without these strategies, it is difficult to achieve deep-blue emission with bipolar materials. However, bipolar

characteristics are necessary in that general polycyclic aromatic hydrocarbon materials have more rapid hole mobility than electron mobility, hindering charge balance maintenance in OLED devices [9,10]. Considering that charge injection and transport in OLED devices are the main factors that affect electroluminescence (EL) performance, bipolar characteristics that facilitate charge injection and movement are required. Additionally, bipolar materials maintain excellent charge balance at high luminance by efficiently generating excitons while exhibiting low roll-off [11]. Yi Jia's group developed a donor-spacer-acceptor-type dopant composed of carbazole and 1H-phenanthro[9,10-d]imidazole, then separated the carbazole and imidazole components by introducing biphenyl as a spacer; non-doped devices with this as-described dopant showed an external quantum efficiency (EQE) of 6.0% and CIE coordinates of (0.16, 0.08) [12]. Jiwon Yoon et al. reported bipolar material fabrication using mCP as the backbone while substituting 2,4-diphenylpyrimidine; a photoluminescence maximum (PLmax) value of 426 nm was observed in the film state for application as a green host, indicating that bipolar characteristics were utilized with excellent charge balance [13]. Jun Ye's group synthesized two materials consisting of a symmetrical D- π -A- π -D structure (CzS1, CzS2); the OLED device using these two materials showed EQEs of 4.2% and 2.7% and CIE coordinates of (0.157, 0.055) and (0.157, 0.44), respectively [14].

In the present study, a novel deep-blue bipolar emitter of the donor-spacer-acceptor type (D- π -A), 9-(4-(4,6-diphenyl-1),3,5-triazin-2-yl)-2,5-dimethylphenyl)-9H-carbazole or DTPCZ, was designed and successfully synthesized. Carbazole (hereinafter, Cz) was used as the donor; Cz is the most commonly used donor moiety because it is cheap and easy to synthesize, and it exhibits excellent hole transport properties. As an acceptor, a bulky diphenyl triazine (hereinafter, Tz) moiety that can effectively prevent packing between molecules was introduced; *p*-xylene was used as the spacer between Cz and Tz. Intramolecular charge transfer was controlled by inducing substantial steric hindrance via the methyl group of *p*-xylene. Additionally, the synthesized material was polymerized via condensation polymerization to confirm the characteristics of the bipolar blue polymer. In the polymer, intramolecular twist was maintained to prevent charge transfer and to realize blue emission, allowing confirmation of the photophysical and EL characteristics.

2. Materials and Methods

The relevant NMR data is presented in Figures S7–S11, and the GPC data for poly DTPCZ is shown in Figure S12.

2.1. Synthesis of 9-(4-Bromo-2,5-dimethyl-phenyl)-9H-carbazole (1)

1,4-Dibromo-2,5-dimethyl-benzene (20 g, 76 mmol), 9H-carbazole (19 g, 114 mmol), copper iodide (CuI) (0.72 g, 3.8 mmol), trans-1,2-cyclohexanediamine (0.92 mL, 7.6 mmol), and potassium phosphate (K₃PO₄) (51 g, 240 mmol) were added to a 500 mL round-bottom flask, followed by nitrogen substitution and connection to a reflux apparatus. After adding 150 mL of 1,4-dioxane, the mixture was stirred at an elevated temperature for 24 h. Upon completion of the reaction, the solvent was removed, and the residue was extracted with CH₂Cl₂ and distilled water. After treatment with MgSO₄ and filtration, the product was obtained by column chromatography using hexane, yielding 52%.

¹H NMR (300 MHz, DMSO-d₆): δ (ppm) 1.80(s, 3H), 2.35(s, 3H), 6.96–6.99(d, J = 8.1, 2H), 7.21–7.26(m, 2H), 7.33–7.38(m, 3H), 7.78(s, 1H), 8.18–8.22(d, J = 9.1, 2H).

2.2. Synthesis of 9-(4-Boronic acid-2,5-dimethyl-phenyl)-9H-carbazole (2)

In a 500 mL three-neck flask, 12 g (34 mmol) of compound (1) was added, followed by the addition of 180 mL of tetrahydrofuran (THF). While maintaining a temperature of –78 °C using dry ice, 26 mL (51 mmol) of *n*-butyllithium (*n*-BuLi) was added, and after approximately 5 min, 6.0 mL (51 mmol) of triethyl borate (B(OEt)₃) was added. Upon completion of the reaction, diluted hydrochloric acid (HCl) was added. The solvent was then removed, and the mixture was extracted with ethyl acetate (EA) and distilled water.

After treatment with MgSO_4 and filtration, the product was re-precipitated using THF and hexane. The yield was 41%.

^1H NMR (300 MHz, DMSO-d_6): δ (ppm) 1.83 (s, 3H), 2.44 (s, 3H), 6.95–6.98 (d, $J = 8.1$, 2H), 7.15 (s, 1H), 7.23–7.28 (m, 2H), 7.37–7.43 (m, 2H), 7.60 (s, 1H), 8.20–8.25 (m, 4H).

2.3. Synthesis of 9-[4-(4,6-Diphenyl-[1,3,5]triazin-2-yl)-2,5-dimethyl-phenyl]-9H-carbazole (DTPCZ)

In a 1000 mL three-neck flask, 4.4 g (14 mmol) of compound (2), 4.5 g (16 mmol) of 2-chloro-4,6-diphenyl-[1,3,5]triazine, and 0.80 g (0.70 mmol) of tetrakis(triphenylphosphine) palladium(0) ($\text{Pd}(\text{PPh}_3)_4$) were added under nitrogen conditions. Then, 360 mL of anhydrous toluene was added, and the temperature was raised to 50 °C. Subsequently, 36 mL of a 2 M potassium carbonate (K_2CO_3) solution was added, and the mixture was refluxed for 5 h. Upon completion of the reaction, the solvent was evaporated, and the residue was extracted with CH_2Cl_2 and distilled water. The resulting solution was treated with MgSO_4 , filtered, and subjected to column chromatography using a mixture of toluene and hexane in a 1:1 ratio. The product was dissolved in THF and reprecipitated with ethanol to yield a 90% yield.

^1H NMR (400 MHz, CDCl_3) δ 8.80–8.75 (m, 4H), 8.39 (s, 1H), 8.18 (ddd, $J = 7.8$, 1.2, 0.7 Hz, 2H), 7.65–7.56 (m, 6H), 7.42 (ddd, $J = 8.3$, 7.1, 1.2 Hz, 2H), 7.39 (s, 1H), 7.30 (ddd, $J = 8.0$, 7.1, 1.0 Hz, 2H), 7.15 (dt, $J = 8.1$, 0.9 Hz, 2H), 2.85 (s, 3H), 2.10 (s, 3H) (Figure S8) ^{13}C NMR (100 MHz, CDCl_3): δ 174.22, 171.61, 141.08, 138.52, 138.31, 136.45, 136.19, 134.88, 134.51, 132.84, 132.43, 129.15, 128.88, 126.10, 123.29, 120.50, 119.82, 110.06, 21.91, 17.52. HRMS (m/z): for $\text{C}_{35}\text{H}_{27}\text{N}_4$: 503.2237[M]⁺. Elemental analysis calculated (%) for $\text{C}_{35}\text{H}_{26}\text{N}_4$: C, 83.64; H, 5.21; N, 11.15. Found: C, 83.23; H, 5.45; N, 11.06.

2.4. Synthesis of 3,6-Dibromo-9-(4-(4,6-diphenyl-1,3,5-triazin-2-yl)-2,5-dimethylphenyl)-9H-carbazole (3)

A total of 0.30 g (0.60 mmol) of DTPCZ and 0.23 g (1.3 mmol) of N-bromosuccinimide (NBS) were added to a 100 mL three-neck round-bottom flask. A total of 20 mL of anhydrous CH_2Cl_2 was added, and the reactants were dissolved. The reaction proceeded for 30 min under a nitrogen atmosphere at room temperature (RT), followed by heating to 50 °C and further reaction for 3 h. After extraction with CH_2Cl_2 /distilled water, moisture was removed by adsorption with MgSO_4 , and the residual solvent was evaporated. Column chromatography using EA and hexane in a 3:7 ratio was performed, and the resulting material was dried to yield a white solid with a 70% yield.

^1H NMR (400 MHz, CDCl_3) δ 8.79–8.74 (m, 4H), 8.36 (s, 1H), 8.23 (dd, $J = 2.0$, 0.5 Hz, 2H), 7.65–7.56 (m, 6H), 7.52 (dd, $J = 8.7$, 1.9 Hz, 2H), 7.34 (s, 1H), 7.01 (dd, $J = 8.7$, 0.6 Hz, 2H), 2.84 (s, 3H), 2.03 (s, 3H).

2.5. Polymerization of Compound (Poly DTPCZ)

A total of 0.38 g (1.4 mmol) of bis(1,5-cyclooctadiene)nickel(0) ($\text{Ni}(\text{COD})_2$) and 0.21 g (1.4 mmol) of 2,2'-bipyridyl were added to a brown 3-neck round-bottom flask. A total of 10 mL of anhydrous dimethylformamide (DMF) solvent was added to dissolve the reactants, followed by the addition of 0.15 g (1.4 mmol) of 1,5-cyclooctadiene (COD), and the temperature was raised to 70 °C. A total of 0.30 g of compound (3) was dissolved in anhydrous toluene and slowly added dropwise to the reaction mixture. After stirring for 72 h, the mixture was cooled to RT. Distilled water and HCl were added to adjust the pH to 7, and the mixture was further stirred for 30 min. After extraction with CH_2Cl_2 /distilled water, solvent removal, and reprecipitation with THF/hexane, a solid product was obtained. (Mn: 3175.1 g/mol, Mw: 4771.6 g/mol).

3. Results and Discussion

Figure 1 shows the chemical structure of the synthesized compounds, Cz and Tz, as the electron donating group and the electron accepting group, respectively; *p*-xylene served as the spacer. The overall synthesis method is presented in Scheme 1, and the

detailed synthesis method is described in the Experimental Section. Monomers were created using the Ullmann reaction, boronic acid synthesis, and Suzuki coupling; polymers were synthesized via Yamamoto polymerization [15–20]. The synthesized materials were purified by a column using silica gel and reprecipitation. The chemical structures of the purified substances were confirmed via proton and carbon-13 nuclear magnetic resonance, fast atom bombardment mass analysis, and gel permeation chromatography.

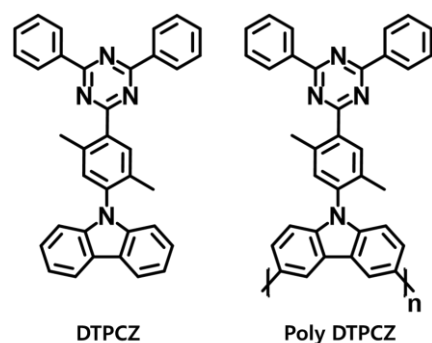
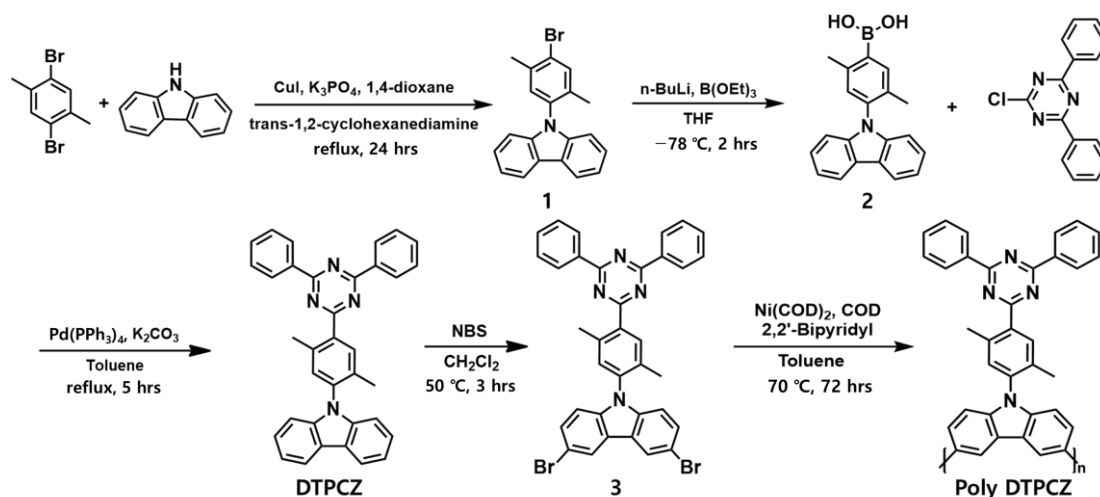


Figure 1. Chemical structures of the newly synthesized compounds.



Scheme 1. Synthetic methods of newly synthesized compounds.

3.1. Optical Properties and Theoretical Calculations

The ultraviolet-visible (UV-Vis) absorption and PL properties of the materials are summarized in Figure 2 and Table 1. The strong absorption bands at approximately 290 nm were assigned to the π - π^* transition of the Cz ring; the weak bands at 310–350 nm correspond to n - π^* transitions of the Cz units. DTPCZ revealed weak and broad absorption bands in the wavelength range of 350–370 nm, which were attributed to intramolecular charge transfer from the Cz donor to the Tz acceptor [21]. The observed behavior was similar to the behavior of the film state. Additionally, through time-dependent density functional theory (TD-DFT), the range of absorption spectra for DTPCZ was investigated. The results showed the largest oscillator strength at 294 nm, indicating the primary absorption peak where the transition from the highest occupied molecular orbital (HOMO)-2 to the lowest unoccupied molecular orbital (LUMO) occurs (Table S1). At this transition, the electron density in HOMO-2 was mainly located in the *p*-xylene moiety and partially in the Cz ring (Figure S1). Also, significant absorptions were observed at 303 and 409 nm, corresponding to transitions from HOMO to LUMO + 2 and from HOMO to LUMO, respectively. In these transitions, the electron density in HOMO was primarily distributed in the Cz ring, with partial localization in the *p*-xylene moiety. Thus, the results confirmed similar absorption characteristics to those observed previously. The PLmax peaks of DTPCZ in the solution

and film states occurred at 421 and 425 nm, respectively. Generally, during the change from a solution state to a film state, the PLmax wavelength was red-shifted and the full width at half maximum (FWHM) was broadened because of the intermolecular interaction caused by the close intermolecular distance. However, FWHM values of 54 and 56 nm were maintained for the solution and film (Figure 2a). The methyl group of the spacer between the donor and the acceptor induced a twist, leading to a dihedral angle of 75.3° between Cz and the spacer (Figure 3). This angle prevented the intramolecular conjugation length from increasing and inhibited intermolecular packing; thus, deep-blue emission was achieved, similar to the emission of the solution, even in the film state [22].

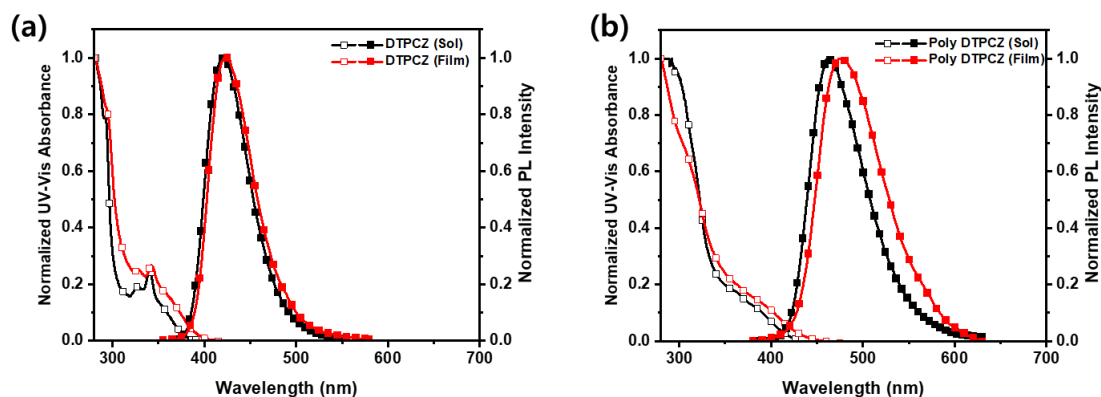


Figure 2. UV-Vis absorption spectra and PL spectra of the synthesized materials: (a) DTPCZ and (b) poly DTPCZ.

Table 1. Optical properties of the synthesized materials.

Compound	Solution ^a			Film ^b			HO MO ^c (eV)	LU MO ^c (eV)	Band Gap ^d (eV)
	λ_{Abs} (nm)	λ_{PL} (FWHM) (nm)	Φ_F ^e (%)	λ_{Abs} (nm)	λ_{PL} (FWHM) (nm)	Φ_F ^e (%)			
DTPCZ	340	421 (54)	43.2	341	425 (56)	18.9	−5.9	−2.8	3.1
Poly DTPCZ	380	461 (68)	32.4	387	475 (84)	9.1	−5.5	−2.6	2.9

^a Toluene solution (0.5 wt%), ^b in thin film state (thickness: 50 nm) for DTPCZ, spin coating film (1 wt% in toluene) for poly DTPCZ; ^c HOMO values derived from ultraviolet photoelectron spectra (Riken-Keiki, AC-2); ^d optical energy band gap (E_g) estimated from the onset of the absorption spectra in a neat film at room temperature; ^e absolute photoluminescence quantum yield.

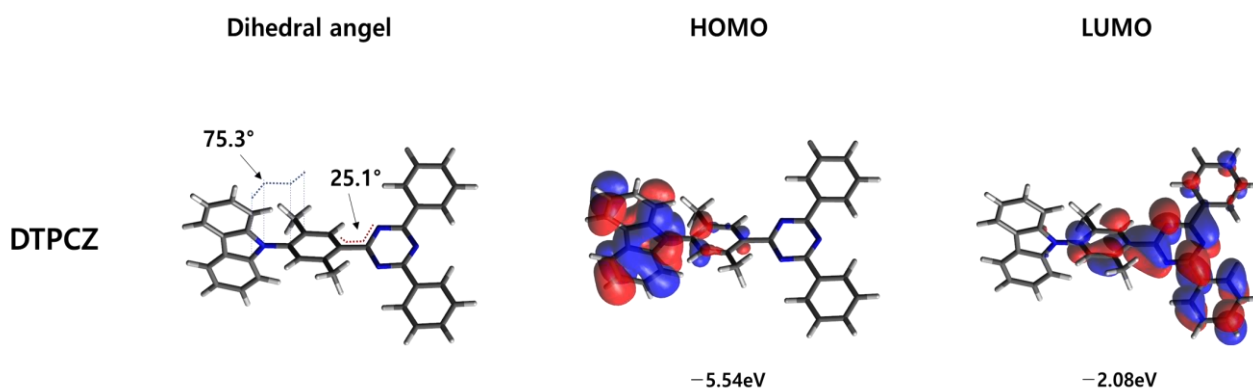


Figure 3. Electron density distributions and dihedral angle of the HOMO and LUMO orbitals of DTPCZ (calculated using the B3LYP/6-31G(d) method).

Poly DTPCZ showed broad absorption in the 300–400-nm range. In the solution state, poly DTPCZ exhibited a PLmax value of 461 nm, while in the film state, it showed a PLmax

value of 475 nm, resulting in red shifts of approximately 40 and 50 nm compared to DTPCZ, respectively. Generally, as the solution/film transitions to a polymer state, the molecular weight increases and the conjugation length becomes longer, resulting in a greater red shift compared with the monomer [23]. However, the difference between the solution and film states of poly DTPCZ itself was observed to be 14 nm, and this characteristic is presumably related to the suppression of intermolecular aggregation via steric hindrance between neighboring molecules in the polymer chain to maintain a stable state [24].

DTPCZ and poly DTPCZ are bipolar materials with a donor-acceptor structure. These materials have distinct optical properties depending on the solvent polarity. There is a slight blue shift of this band with increasing solvent polarity in absorption, which is a typical behavior of $n-\pi^*$ transitions [25,26]. Also, they exhibited similar absorption spectra and shapes overall (Figure S2). However, the PL spectra were red-shifted according to increases in solvent polarity (Figure 4). As shown in Figure 4 and Table 2, the peak of the PL spectra of DTPCZ varied from 397 nm for hexane to 522 nm for dimethyl sulfoxide (DMSO); the FWHM broadened from 44 to 111 nm, respectively. Notably, hexane and DMSO have dielectric constants of 1.9 and 46.7, respectively. Poly DTPCZ was not soluble in hexane; thus, the PL spectrum could not be measured. The PLmax shifted from 466 nm for toluene (dielectric constant: 2.38) to 559 nm for DMSO, respectively; the FWHM broadened from 71 to 125 nm. The PL wavelength of DTPCZ and poly DTPCZ exhibited a red shift in polar solvents because bipolar molecules are influenced by the solvation effect, which stabilizes with increasing solvent polarity in the excited state. From toluene to DMSO, DTPCZ shifted by 101 nm, and poly DTPCZ shifted by 89 nm. Poly DTPCZ was expected to exhibit a greater shift; however, as described above, steric hindrance with neighboring molecules in the polymer may have prevented large shifts in the PL spectra. As the polarity of the solvent increases, the PL emission shifts to longer wavelengths. This is because, in the ground state, the molecule's dipole moment is not influenced by the solvent polarity, resulting in similar absorption peaks. However, in the excited state, the molecule is affected by both the generated charge within the molecule and the solvent polarity. As a result, as the dielectric constant of the solvent increases, the molecule interacts more with the dipole of the solvent, stabilizing the excited state and reducing the band gap, leading to a gradual red shift in the PL max value [27].

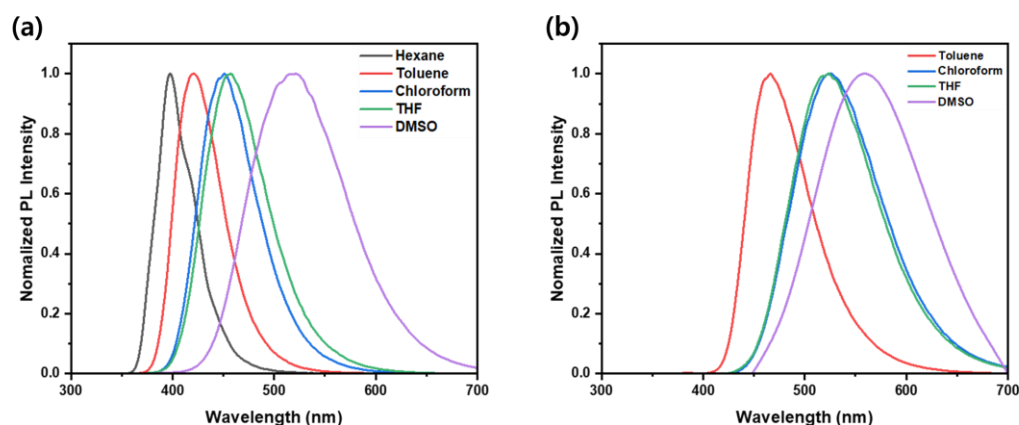


Figure 4. PL spectra of synthesized bipolar materials in different solvents at 0.5 wt%: (a) DTPCZ, (b) poly DTPCZ.

The photoluminescence quantum yields (PLQY) values of DTPCZ were 43.2% in the solution state and 18.9% in the film state. The PLQY values of poly DTPCZ were 32.4% in the solution state and 9.1% in the film state. As shown in Table 1, there is a difference of about 4 nm in the PL wavelength between the solution and the film of DTPCZ. This could be due to the minimization of intermolecular packing with the introduction of the spacer. If intermolecular packing had not been prevented, the PL value in the film would have shown a further red shift or exhibited peaks in the excimer form. Nevertheless, the

decrease in PLQY value in the film is a common phenomenon observed when all materials are converted from solution to film state, and it is interpreted that the effect of preventing intermolecular packing by the methyl group of DTPCZ did not fully resolve this issue. In the solution state, the decrease in the PLQY value between DTPCZ and poly DTPCZ was small. This characteristic can be attributed to the introduction of bulky Tz with an intramolecular dihedral angle of 75.3° , which allowed a similar structure to be maintained in polymer form. This finding is also consistent with the solvatochromism results of poly DTPCZ. Additionally, transient photoluminescence decay measurements were conducted to confirm the thermally activated delayed fluorescence (TADF) characteristics. A tau value of $0.86 \mu\text{s}$ was observed, and delayed fluorescence was not detected (Figure S3).

Table 2. PLmax wavelength of DTPCZ and poly DTPCZ in hexane, toluene, chloroform, THF, and DMSO solvent (concentration: 0.5 wt%).

	PLmax (nm)				
	Hexane (1.88) ^a	Toluene (2.38) ^a	Chloroform (4.81) ^a	THF (7.58) ^a	DMSO (46.7) ^a
DTPCZ	397	421	451	457	522
Poly DTPCZ	NA ^b	466	526	524	559

^a Dielectric constant of each solvent. ^b not available.

Highest occupied molecular orbital (HOMO) values were measured by ultraviolet photoelectron spectroscopy (Riken-Keiki, AC-2); optical band gaps were derived from the absorption edge in plots of $h\nu$ versus $(\alpha h\nu)^2$, where α , h , and ν are the absorbance, Planck's constant, and the frequency of light, respectively. The respective HOMO levels of DTPCZ and poly DTPCZ were -5.9 and -5.5 eV; the corresponding lowest unoccupied molecular orbital (LUMO) levels were -2.8 and -2.6 eV. Consistent with density functional theory, the electron density of DTPCZ was mainly distributed in Cz of the donating group in the HOMO, and in Tz of the accepting group in the LUMO (Figure 3). Thus, charge transfer could occur, leading to a reduction in the band gap of DTPCZ. Compared with the monomer, the polymer had a shallow HOMO level and a small band gap because of its longer conjugated length.

3.2. Thermal Properties

To confirm the thermal stability and properties of the synthesized materials, thermogravimetric (TGA) analysis and differential scanning calorimetry (DSC) measurements were conducted; the results are shown in Figure 5. The decomposition temperatures (T_d , corresponding to 5% weight loss) values of DTPCZ and poly DTPCZ were measured at 349°C and 445°C , respectively. The glass transition temperature (T_g) of DTPCZ was 108°C , and the melting temperature (T_m) was 220°C . The T_g of poly DTPCZ was 153°C . Therefore, DTPCZ and poly DTPCZ demonstrated high thermal stability, indicating their capacity to enable stable operation of OLED devices [28].

3.3. Electroluminescence Properties

Non-doped devices and 10-, 20-, and 30-wt% doped OLED devices were fabricated using the newly synthesized DTPCZ as a dopant for the emitting layer. The non-doped device had the following configuration: indium tin oxide (ITO)/dipyrazino[2,3-f:2',3'-h] quinoxaline-2,3,6,7,10,11-hexacarbonitrile (HATCN) (5 nm)/N,N'-bis(naphthalene-1-yl)-N,N'-bis(phenyl)benzidine (NPB) (40 nm)/4,4',4'-Tris(carbazol-9-yl)triphenylamine (TCTA) (5 nm)/DTPCZ (20 nm)/1,3,5-tri(1-phenyl-1H-benzo[d]imidazole-2-yl) phenyl (TPBi) (40 nm)/LiF (1 nm)/Al (200 nm). The doped device was fabricated with the configuration of ITO/HAT-CN (5 nm)/NPB (40 nm)/TCTA (5 nm)/4,4'-Bis(N-carbazolyl)-1,1'-biphenyl (CBP): 10-, 20-, or 30-wt% DTPCZ (20 nm)/TPBi (40 nm)/LiF (1 nm)/Al (200 nm). HATCN was used as the hole-injection layer, and NPB was used as the hole transporting layer. TCTA served as the exciton blocking layer, TPBi served as the electron-transporting

layer and hole-blocking layer, and LiF and Al served as the electron-injecting material and the cathode, respectively.

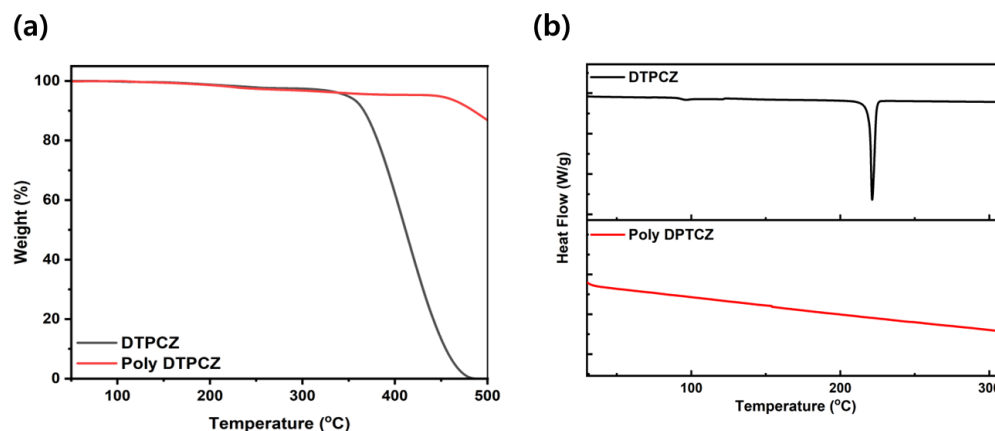


Figure 5. Thermal properties of DTPCZ and poly DTPCZ: (a) TGA analysis and (b) DSC results.

The fabricated non-doped device had an operation voltage of 4.0 V at 10 mA/cm² and showed low efficiency; specifically, it had a current efficiency (CE) of 1.64 cd/A, a power efficiency (PE) of 1.11 lm/W, and an external quantum efficiency (EQE) of 1.63% (Figure 6). The ELmax peak was observed at 423 nm, similar to the PL peak of the DTPCZ film. However, the CIE coordinates were measured as (0.18, 0.17); emission over the 500–600-nm range was observed in the EL spectrum, which was not visible in the film PL. These results indicate a problem whereby the recombination zone within the device occurs at the interface between DTPCZ and the neighboring TCTA. Upon examining the energy band diagram of the device, it is observed that there is almost no energy barrier for electrons to move from TPBi to EML via the LUMO. However, a significant energy barrier of 0.23 eV exists for holes to move from TCTA to EML via the HOMO (Figure 6f). Therefore, by varying the thickness and type of the hole carrier transport layer, we aim to shift the position of the recombination zone in the center of the emitting layer. We will observe the resulting performance changes and report them separately in the future.

In order to match the carrier balance, a doped device was fabricated. Figure 7a–d shows the determined current density (J)–voltage (V)–luminance (L) curve, the CE, the EL spectra according to doping concentration, and the band diagram of the doped devices, respectively. The EL performances of the devices are summarized in Table 3. The operating voltage of the three fabricated devices was consistently low at 3.9 V. Among them, when DTPCZ was doped at a concentration of 20 wt%, it exhibited the highest EL performance with a CE of 1.17 cd/A, an EQE of 2.32%, and a PE of 0.68 lm/W (Figure S4). When doped at 10 wt%, the low dopant concentration resulted in insufficient energy transfer from the host to the dopant, leading to lower efficiency. According to the increase in doping concentration from 20 to 30 wt%, all EL efficiencies showed a decrease. This result occurred because the luminescence efficiency was reduced by the aggregation quenching effect at high doping concentrations [29,30]. Additionally, all fabricated devices adequately maintained their carrier balance, even at high luminance, beginning at 20 mA/cm²; the maximum CE was 50 mA/cm², and the current density was high. The 10 wt% doped devices showed only a slight roll-off effect. The roll-off values of devices doped with 20 and 30 wt% showed 9.0% and 6.9%, respectively (Figure 7b). The small roll-off of less than 10% observed in these materials is a key characteristic of materials with bipolar properties, as it helps maintain carrier balance within the device. To further confirm this, hole-only devices (HOD) and electron-only devices (EOD) of DTPCZ were fabricated. The structures of HOD and EOD are as follows: ITO/molybdenum trioxide (MoO₃) (1 nm)/EML (50 nm)/MoO₃ (10 nm)/Al (100 nm) and ITO/TPBi (40 nm)/EML (50 nm)/TPBi (40 nm)/LiF (1 nm)/Al (100 nm). As a result, it was confirmed that the mobility of both holes and electrons was similar, exhibiting good bipolar characteristics (Figure S5). All doped devices showed the same ELmax peak

of 430 nm and a FWHM value of 61 nm. The CIE values were identical (0.16, 0.06) in 10- and 20-wt%-doped devices; however, the CIE y-value increased to (0.17, 0.09) in the 30 wt% doped device. Therefore, a doping concentration of 20 wt% provided the optimal results and showed the highest EL efficiency, as well as a CIE y-value of deep-blue emission—this was better than the mobile specification value of approximately 0.15 while satisfying the television specification value of 0.08 [31,32]. Moiety composed of donor-acceptor types, such as DTPCZ, exhibits TADF properties and can also demonstrate high OLED efficiency. However, in the case of DTPCZ, it does not possess TADF characteristics and showed low efficiency due to exciplex in the non-doped device structure. Nonetheless, by utilizing a doping system, we enhanced EQE by approximately 1.4 times. We will report on the synthesis of various new derivatives in the future.

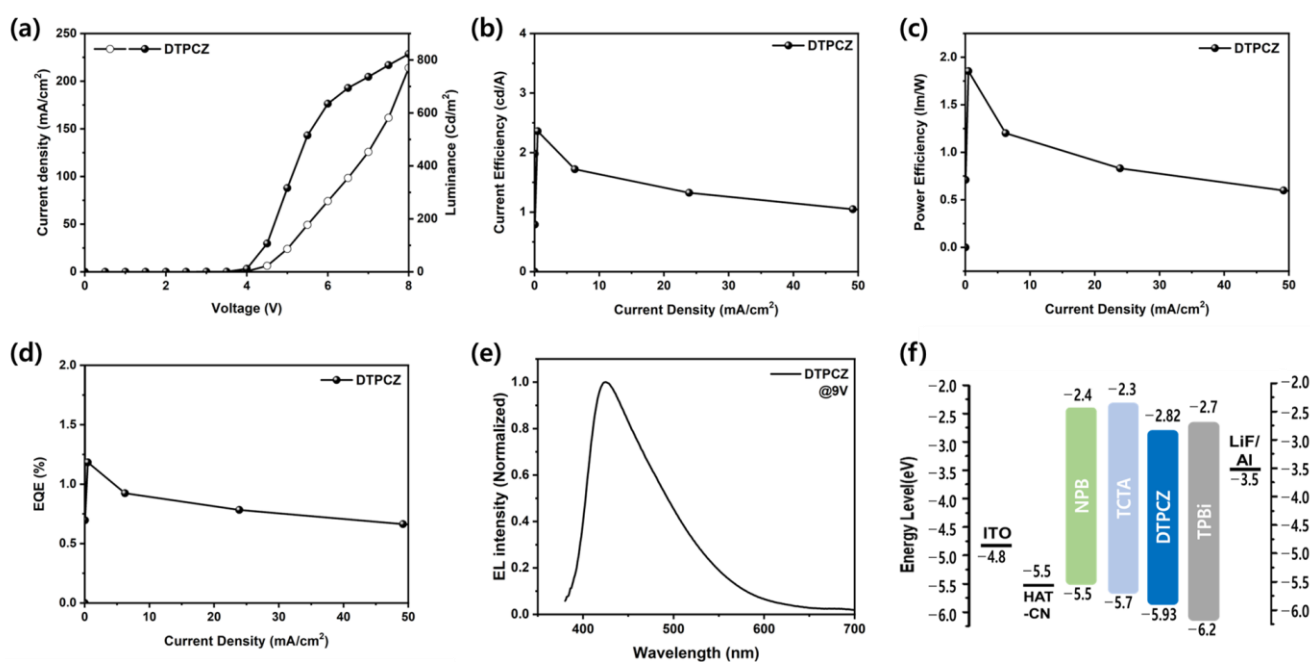


Figure 6. EL characteristics of non-doped DTPCZ devices: (a) J-V-L curve, (b) CE versus current density, (c) PE versus current density, (d) EQE versus current density, (e) EL spectrum at 9.0 V, and (f) the band diagram of the materials in OLED devices.

Table 3. EL performances of doped OLED devices at 10 mA/cm².

@ 10 mA/cm ²	V _{on} ^a (V)	CE (cd/A)	EQE (%)	PE (lm/W)	EL _{max} (nm)	FWHM (nm)	CIE (x, y)
CBP: 10% DTPCZ	3.9	0.48	1.07	0.30	430	61	(0.16, 0.06)
CBP: 20% DTPCZ	3.9	1.17	2.32	0.68	430	61	(0.16, 0.06)
CBP: 30% DTPCZ	3.9	0.97	2.05	0.59	430	61	(0.17, 0.09)

^a Operating voltage of 10 mA/cm².

Polymer deposition devices could not be manufactured because of their high molecular weight. Thus, OLEDs were fabricated using a solution process. The devices were fabricated with the configuration ITO/poly(2,3-dihydrothieno-1,4-dioxin):polystyrene sulfonate (PEDOT:PSS) (40 nm)/CBP: 5 wt% poly DTPCZ (20 nm)/TPBi (40 nm)/LiF (1 nm)/Al (200 nm). PEDOT:PSS was included for hole injection, and CBP was used as the host material. TPBi was used as an electron-transporting and hole-blocking layer (Figure S6a). As shown in the J-V curves, the device operated normally, and the EL maximum peaks occurred at 465 nm, with energy transfer from the host to the dopant (Figure S6b,c). However, because of the low PLQY of poly DTPCZ, EQE_{max} exhibited a low device efficiency of approximately 0.6%. Further improvements in device fabrication for both DTPCZ and poly DTPCZ are

possible by optimizing the solution process and the device structure. The synthesized DTPCZ facilitated the fabrication of both non-doped and doped devices, and poly DTPCZ based on this material allowed device fabrication via solution processing. Materials such as DTPCZ play a significant role in organic semiconductors due to their versatility across various fields and components.

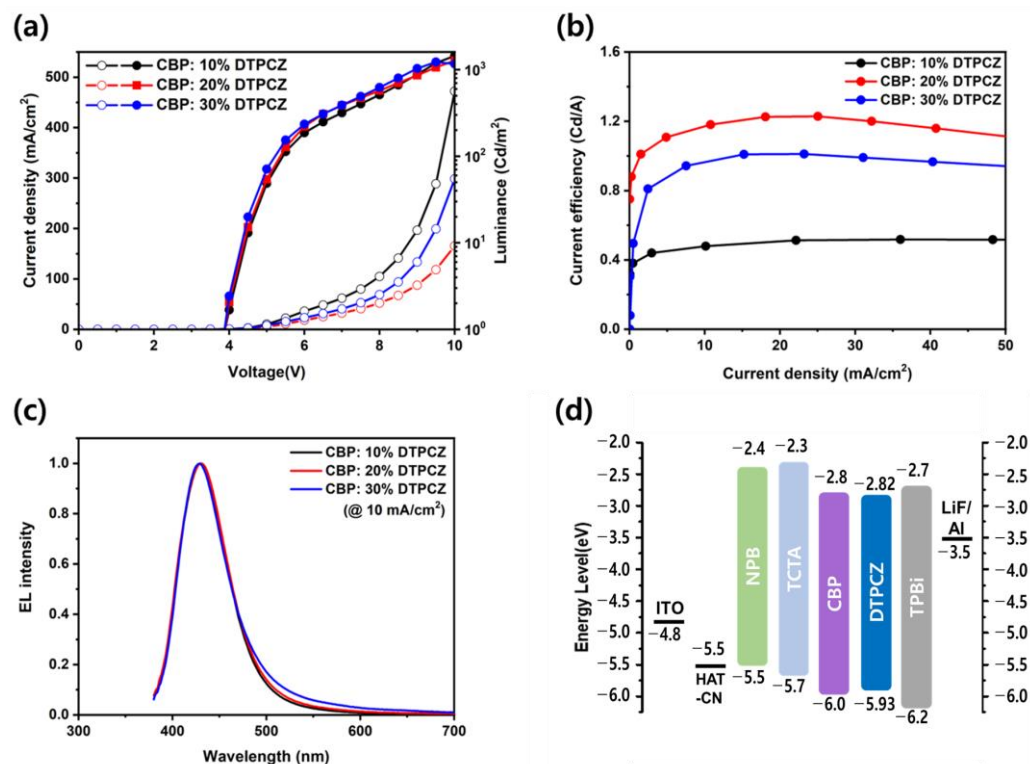


Figure 7. EL characteristics of DTPCZ devices as emission layers (EMLs) with respect to the dopant concentration: (a) J-V-L curves, (b) luminance efficiency versus current density, (c) EL spectra doped devices, and (d) band diagram of the materials in OLED devices.

4. Conclusions

To realize an efficient deep-blue OLED device, a donor-spacer-acceptor-type of DTPCZ with bipolar characteristics was successfully synthesized; its characteristics were confirmed. Cz was used as the donor, a Tz moiety was introduced as the acceptor, and a *p*-xylene group was adopted as the spacer to control the twisted structure of the molecule, as well as the electron densities of the HOMO and LUMO levels. When DTPCZ was applied to the EL-doped device, a CE of 1.2 cd/A, an EQE of 2.3%, and a PE of 0.7 lm/W were achieved. Additionally, the CIE *y*-value was 0.06, which is near the 0.08 value specified for OLED televisions and required for the development of deep-blue device platforms. In the future, it will be possible to develop many bipolar derivatives by using the strategies proposed in this study for deep-blue material design. Furthermore, this molecular design approach is applicable to various fields, including organic semiconductors.

Supplementary Materials: The following supporting information can be downloaded at: <https://www.mdpi.com/article/10.3390/app14093593/s1>, Table S1: Absorption frequencies and oscillator strengths calculated with TD-B3LYP/6-311G(d) for the DTPCZ; Figure S1: Electron density distributions of molecular orbitals of DTPCZ (calculated using the B3LYP/def2-TZVP method); Figure S2: Normalized UV-Vis absorption spectra of (a) DTPCZ and (b) poly DTPCZ according to different polarities of solvents at 0.5 wt%; Figure S3: Transient photoluminescence decay spectra of the solution (toluene) (IRF: instrument response function), range: 100 μ s; Figure S4: EL characteristics of devices using DTPCZ as an EML dopant: (a) power efficiency versus current density, and (b) external quantum efficiency versus current density; Figure S5: J-V characteristics of HOD and EOD of DTPCZ; Figure S6:

EL characteristics of devices using poly DTTPCZ as EMLs (5 wt% dopant): (a) band diagram of the solution process OLED device, (b) J-V curve, and (c) EL spectrum of the doped device of poly DTTPCZ; Figure S7: ^1H NMR spectra of compound (1) recorded in DMSO-d_6 (300 MHz); Figure S8: ^1H NMR spectra of compound (2) recorded in DMSO-d_6 (300 MHz); Figure S9: ^1H NMR spectra of DTTPCZ recorded in CDCl_3 (400 MHz); Figure S10: ^{13}C NMR spectra of DTTPCZ recorded in CDCl_3 (100 MHz); Figure S11: ^1H NMR spectra of compound (3) recorded in CDCl_3 (400 MHz); Figure S12: GPC traces of synthesized poly DTTPCZ using THF as eluent.

Author Contributions: Conceptualization, S.J. and J.P.; methodology, H.K.; validation, H.L. and J.P.; formal analysis, K.L.; investigation, S.P. and H.K.; resources, J.P.; writing—original draft preparation, S.J., S.P. and J.P.; writing—review and editing, H.L., K.L. and J.P.; visualization, S.J., S.P. and H.K.; supervision, J.P.; project administration, J.P.; funding acquisition, J.P. All authors have read and agreed to the published version of the manuscript.

Funding: This work was supported by the GRRRC program of Gyeonggi province. [(GRRCKYUNGHEE2023-B01), Development of ultra-fine process materials based on the sub-nanometer class for next-generation semiconductors].

Institutional Review Board Statement: Not applicable.

Informed Consent Statement: Not applicable.

Data Availability Statement: Data are contained within the article and Supplementary Materials.

Conflicts of Interest: The authors declare no conflicts of interest.

References

1. Kang, S.; Jung, H.; Lee, H.; Park, S.; Kim, J.; Park, J. Highly efficient dual-core derivatives with EQEs as high as 8.38% at high brightness for OLED blue emitters. *J. Mater. Chem. C* **2019**, *7*, 14709–14716. [[CrossRef](#)]
2. Ashok Kumar, S.; Shankar, J.S.; Periyasamy, B.K.; Nayak, S.K. Device engineering aspects of Organic Light-Emitting Diodes (OLEDs). *Polym.-Plast. Technol. Mater.* **2019**, *58*, 1597–1624. [[CrossRef](#)]
3. Kim, H.J.; Kang, H.; Jeong, J.E.; Park, S.H.; Koh, C.W.; Kim, C.W.; Woo, H.Y.; Cho, M.J.; Park, S.; Choi, D.H. Ultra-Deep-Blue Aggregation-Induced Delayed Fluorescence Emitters: Achieving Nearly 16% EQE in Solution-Processed Nondoped and Doped OLEDs with CIE $y < 0.1$. *Adv. Funct. Mater.* **2021**, *31*, 2102588. [[CrossRef](#)]
4. Reddy, S.S.; Sree, V.G.; Cho, W.; Jin, S.H. Achieving Pure Deep-Blue Electroluminescence with CIE $y \leq 0.06$ via a Rational Design Approach for Highly Efficient Non-Doped Solution-Processed Organic Light-Emitting Diodes. *Chem. Asian J.* **2016**, *11*, 3275–3282. [[CrossRef](#)] [[PubMed](#)]
5. Hung, W.-Y.; Chi, L.-C.; Chen, W.-J.; Chen, Y.-M.; Chou, S.-H.; Wong, K.-T. A new benzimidazole/carbazole hybrid bipolar material for highly efficient deep-blue electrofluorescence, yellow–green electrophosphorescence, and two-color-based white OLEDs. *J. Mater. Chem.* **2010**, *20*, 10113–10119. [[CrossRef](#)]
6. Peng, L.; Huo, Y.; He, S.; Liu, Y.; Ren, Z.; Ying, S.; Yan, S. A linear deep-blue bipolar fluorescent material with the CIE $y < 0.065$ serving as the emitter and host for high-performance monochromatic and hybrid white OLEDs. *J. Mater. Chem. C* **2022**, *10*, 11642–11653. [[CrossRef](#)]
7. Tan, Y.; Zhao, Z.; Shang, L.; Liu, Y.; Wei, C.; Li, J.; Wei, H.; Liu, Z.; Bian, Z.; Huang, C. A novel bipolar D– π –A type phenanthroimidazole/carbazole hybrid material for high efficiency nondoped deep-blue organic light-emitting diodes with NTSC CIE y and low efficiency roll-off. *J. Mater. Chem. C* **2017**, *5*, 11901–11909. [[CrossRef](#)]
8. Kim, M.K.; Kwon, J.; Kwon, T.-H.; Hong, J.-I. A bipolar host containing 1,2,3-triazole for realizing highly efficient phosphorescent organic light-emitting diodes. *New J. Chem.* **2010**, *34*, 1317–1322. [[CrossRef](#)]
9. Zhang, D.; Duan, L. Polycyclic Aromatic Hydrocarbon Derivatives toward Ideal Electron-Transporting Materials for Organic Light-Emitting Diodes. *J. Phys. Chem. Lett.* **2019**, *10*, 2528–2537. [[CrossRef](#)]
10. Chi, C.-C.; Chiang, C.-L.; Liu, S.-W.; Yueh, H.; Chen, C.-T.; Chen, C.-T. Achieving high-efficiency non-doped blue organic light-emitting diodes: Charge-balance control of bipolar blue fluorescent materials with reduced hole-mobility. *J. Mater. Chem.* **2009**, *19*, 5561–5571. [[CrossRef](#)]
11. Yu, P.; Xiao, Y. Non-Doped Deep-Blue OLEDs Based on Carbazole-pi-Imidazole Derivatives. *Materials* **2021**, *14*, 2349. [[CrossRef](#)] [[PubMed](#)]
12. Jia, Y.; Zhang, Y.; Fan, S.; Wu, S.; Zhao, X.; Wang, S.; Li, X. A novel bipolar carbazole/phenanthroimidazole derivative for high efficiency nondoped deep-blue organic light-emitting diodes. *Org. Electron.* **2019**, *64*, 259–265. [[CrossRef](#)]
13. Yoon, J.; Lee, C.; Park, S.H.; Kang, D.W.; Kim, H.; Jeong, J.-E.; Woo, H.Y.; Hong, C.S.; Park, S.; Cho, M.J.; et al. Pyrimidine-based bipolar host materials for high efficiency solution processed green thermally activated delayed fluorescence OLEDs. *J. Mater. Chem. C* **2020**, *8*, 2196–2204. [[CrossRef](#)]

14. Ye, J.; Chen, Z.; Fung, M.-K.; Zheng, C.; Ou, X.; Zhang, X.; Yuan, Y.; Lee, C.-S. Carbazole/Sulfone Hybrid D- π -A-Structured Bipolar Fluorophores for High-Efficiency Blue-Violet Electroluminescence. *Chem. Mater.* **2013**, *25*, 2630–2637. [[CrossRef](#)]
15. Suzuki, K.; Kubo, S.; Shizu, K.; Fukushima, T.; Wakamiya, A.; Murata, Y.; Adachi, C.; Kaji, H. Triarylboron-Based Fluorescent Organic Light-Emitting Diodes with External Quantum Efficiencies Exceeding 20. *Angew. Chem. Int. Ed. Engl.* **2015**, *54*, 15231–15235. [[CrossRef](#)]
16. Chen, C.-H.; Huang, W.-S.; Lai, M.-Y.; Tsao, W.-C.; Lin, J.T.; Wu, Y.-H.; Ke, T.-H.; Chen, L.-Y.; Wu, C.-C. Versatile, Benzimidazole/Amine-Based Ambipolar Compounds for Electroluminescent Applications: Single-Layer, Blue, Fluorescent OLEDs, Hosts for Single-Layer, Phosphorescent OLEDs. *Adv. Funct. Mater.* **2009**, *19*, 2661–2670. [[CrossRef](#)]
17. Gibson, V.C.; Spitzmesser, S.K.; White, A.J.; Williams, D.J. Synthesis and reactivity of 1, 8-bis (imino) carbazolide complexes of iron, cobalt and manganese. *Dalton Trans.* **2003**, *13*, 2718–2727. [[CrossRef](#)]
18. Miyaura, N.; Suzuki, A. Palladium-catalyzed cross-coupling reactions of organoboron compounds. *Chem. Rev.* **1995**, *95*, 2457–2483. [[CrossRef](#)]
19. Orecchia, P.; Petkova, D.S.; Goetz, R.; Rominger, F.; Hashmi, A.S.K.; Schaub, T. Pd-Catalysed Suzuki–Miyaura cross-coupling of aryl chlorides at low catalyst loadings in water for the synthesis of industrially important fungicides. *Green. Chem.* **2021**, *23*, 8169–8180. [[CrossRef](#)]
20. Zhang, Z.-B.; Fujiki, M.; Tang, H.-Z.; Motonaga, M.; Torimitsu, K. The first high molecular weight poly (N-alkyl-3, 6-carbazole). *Macromolecules* **2002**, *35*, 1988–1990. [[CrossRef](#)]
21. Li, H.; Li, J.; Liu, D.; Huang, T.; Li, D. Effects of Electron Affinity and Steric Hindrance of the Trifluoromethyl Group on the π -Bridge in Designing Blue Thermally Activated Delayed Fluorescence Emitters. *Chem. Eur. J.* **2020**, *26*, 6899–6909. [[CrossRef](#)] [[PubMed](#)]
22. Wu, H.T.; Yao, Z.F.; Xu, Z.; Kong, H.K.; Wang, X.Y.; Li, Q.Y.; Wang, J.Y.; Pei, J. Controlling Solution-State Aggregation and Solid-State Microstructures of Conjugated Polymers by Tuning Backbone Conformation. *Macromol. Rapid Commun.* **2022**, *43*, e2200069. [[CrossRef](#)] [[PubMed](#)]
23. Zong, W.; Qiu, W.; Yuan, P.; Wang, F.; Liu, Y.; Xu, S.; Su, S.J.; Cao, S. Thermally activated delayed fluorescence polymers for high-efficiency solution-processed non-doped OLEDs: Convenient synthesis by binding TADF units and host units to the pre-synthesized polycarbazole-based backbone via click reaction. *Polymer* **2022**, *240*, 124468. [[CrossRef](#)]
24. Huang, T.; Jiang, W.; Duan, L. Recent progress in solution processable TADF materials for organic light-emitting diodes. *J. Mater. Chem. C* **2018**, *6*, 5577–5596. [[CrossRef](#)]
25. Usta, H.; Risko, C.; Wang, Z.; Huang, H.; Deliomeroğlu, M.K.; Zhukhovitskiy, A.; Facchetti, A.; Marks, T.J. Design, Synthesis, and Characterization of Ladder-Type Molecules and Polymers. Air-Stable, Solution-Processable n-Channel and Ambipolar Semiconductors for Thin-Film Transistors via Experiment and Theory. *J. Am. Chem. Soc.* **2009**, *131*, 5586–5608. [[CrossRef](#)] [[PubMed](#)]
26. Karelson, M.; Zerner, M.C. On the n- π * blue shift accompanying solvation. *J. Am. Chem. Soc.* **1990**, *112*, 9405–9406. [[CrossRef](#)]
27. Jung, H.; Shin, H.; Kim, S.; Kim, J.; An, B.-K.; Lee, J.-H.; Ihee, H.; Park, J. High electroluminescence efficiency and long device lifetime of a fluorescent green-light emitter using aggregation-induced emission. *J. Ind. Eng. Chem.* **2020**, *87*, 213–221. [[CrossRef](#)]
28. Kang, S.; Jung, H.; Lee, H.; Lee, S.; Jung, M.; Lee, J.; Kim, Y.C.; Park, J. Blue light emission of new anthracene derivatives produced using optimized side group link positions. *Dye. Pigment.* **2018**, *156*, 369–378. [[CrossRef](#)]
29. Yang, T.; Liang, B.; Cheng, Z.; Li, C.; Lu, G.; Wang, Y. Construction of Efficient Deep-Red/Near-Infrared Emitter Based on a Large π -Conjugated Acceptor and Delayed Fluorescence OLEDs with External Quantum Efficiency of over 20%. *J. Phys. Chem. C* **2019**, *123*, 18585–18592. [[CrossRef](#)]
30. Wu, C.; Liu, W.; Li, K.; Cheng, G.; Xiong, J.; Teng, T.; Che, C.M.; Yang, C. Face-to-Face Orientation of Quasipolar Donor and Acceptor Enables Highly Efficient Intramolecular Exciplex Fluorescence. *Angew. Chem. Int. Ed.* **2021**, *60*, 3994–3998. [[CrossRef](#)]
31. Tao, S.; Lee, C.S.; Lee, S.-T.; Zhang, X. Efficient blue and white organic light-emitting devices based on a single bipolar emitter. *Appl. Phys. Lett.* **2007**, *91*, 013507. [[CrossRef](#)]
32. Lee, J.-H.; Tsai, H.-H.; Leung, M.-K.; Yang, C.-C.; Chao, C.-C. Phosphorescent organic light-emitting device with an ambipolar oxadiazole host. *Appl. Phys. Lett.* **2007**, *90*, 243501. [[CrossRef](#)]

Disclaimer/Publisher’s Note: The statements, opinions and data contained in all publications are solely those of the individual author(s) and contributor(s) and not of MDPI and/or the editor(s). MDPI and/or the editor(s) disclaim responsibility for any injury to people or property resulting from any ideas, methods, instructions or products referred to in the content.